Journal of
Ceramic Science
and Technology

Effect of Repeated Firing on the Resistance of Screen-Printed Thick-Film Conductors

D. Ortolino, A. Engelbrecht, H. Lauterbach, M. Bräu, J. Kita, R. Moos[*]

Department of Functional Materials, University of Bayreuth, Germany
received July 24, 2014; received in revised form October 1, 2014; accepted October 6, 2014

Abstract

In this paper, the effect of repeated sintering cycles on the resistance of four different thick-film conductor pastes was investigated. Silver, gold, silver-platinum and silver-palladium pastes are widely used in thick-film technology. Their electrical resistance (R) and their temperature coefficient of resistance (TCR) are important material properties. Screen-printed metallization layers were fired repeatedly and their electrical resistance was measured simultaneously during heating and cooling. It was found that the resistances change with increasing number of firing steps and that they run asymptotically to a final value. Light-optical and SEM-EDX analyses explained this behavior. Inorganic compounds of the paste diffuse into the ceramic substrate. The diffusion follows a parabolic diffusion law. A strong correlation between material diffusion and resistance change is found.

Keywords: Thick-film, screen-printing, conductor, gold, silver, silver-palladium, silver-platinum, resistance, TCR, temperature cycling, firing, sintering, material diffusion

I. Introduction

Thick-film hybrid technology is used in many areas of electronic packaging and interconnection technology, especially for harsh environments [1,2,3]. For automotive applications, control devices that have to withstand temperature cycling between -40 °C and 150 °C are often manufactured in thick-film technology [4,5,6]. Sensors installed in the hot exhaust are made of ceramic thick films as well [7,8]. Thick-film technology is a process in which passive elements are applied by means of screen printing onto ceramic substrates. The substrate material for standard applications is 96 % Al_2O_3. The printed layers include conductor tracks, contact pads for components, insulation layers, crossovers, resistors and vias. Almost all of them are sintered at a peak temperature of 850 °C in oxidizing (air) atmosphere in tunnel furnaces. Depending on the application, gold- and silver-based pastes are common for the production of conductor lines, contact pads, and vias. Gold pastes are applied predominantly pure, silver-based pastes are applied both pure and alloyed with platinum or palladium. With this addition, the electromigration of silver is counteracted and the adhesion properties between pastes and substrate are improved [9,10,11,12]. In addition to the metallic components (metal particles, particle size of 0.5 microns – 10 microns), screen-printing pastes for hybrid technology consist of solution and wetting agents, organic binders, additives to adjust the rheological properties and glass frits to provide the mechanical interlock between the paste and the substrate [13]. The proportion of metal particles is between 50 % and 70 %, of organics

between 12 % and 25 % and the proportion of glass frit is 10 % – 20 % [14].

All components are produced in a consecutive way, i.e. the hybrid circuits are usually sintered after each printing step. This means that the first manufactured metallization layers are sintered repeatedly up to more than ten times. Since the proportion of the glass frit is up to 20 %, a change of the properties of the printing layers can be expected, assuming diffusion of the different paste components into the ceramic and the compaction of the thick films, whereas film thicknesses and porosities are decreasing. Cattaneo *et al.*, for instance, investigated how silver migration into end terminations of thick-film resistors affected their electrical properties [15]. The compaction of glass-bonded silver thick films during single sintering in dependence of the glass content has been studied by Yajima and Yamaguchi [16,17].

It is also well known that the morphology of the powders from which the pastes are produced, surfactants, as well as the sintering conditions strongly affect the properties of the printed, dried and fired films [18,19,20]. Studies on the operation of the thick-film hybrids are also published in literature. In [21], for instance, the long-term stability of passive thick-film and LTCC components at elevated temperature up to 500 °C was investigated. Furthermore, failure mechanisms in thick-film materials at 300 °C were examined. The importance of testing the materials under operating conditions was highlighted in this study [22]. The electromigration phenomenon under voltage bias has also been studied at temperatures up to 300 °C [23].

This work does not deal with operation conditions. Rather, the effects of processing are at the center of this study, namely the effect of repeated sintering cycles on

* Corresponding author: functional.materials@uni-bayreuth.de

the electrical properties, in particular on the resistance and on the temperature coefficient of resistance (*TCR*) of four commercial conductor pastes being used in thick-film technology as shown in Table 1. Ag is a pure silver paste, Au a pure gold paste, AgPt and AgPd are alloyed silver pastes with platinum and palladium, respectively.

A pure thick silver paste, a pure gold paste, a silver-platinum paste with a Ag:Pt weight ratio of 100:1 and a silver-palladium paste with a Ag:Pd ratio of 2.5:1 (in respect of the noble metal masses) were studied. Furthermore, the diffusion depths of paste components into the ceramic substrates were determined using SEM images and EDX measurements and the obtained results were correlated with the resistance measurements.

II. Experimental

For all studies conducted in this work, screen-printed test structures according to DIN 41580 – 2 were used (Fig. 1). Each sample consisted of two test structures with four different line widths from 100 µm to 500 µm and three different spaces from 150 µm to 300 µm. In this study only the widest conductor with 500 µm was investigated, as can be seen in Fig. 1. To prepare the test structures on 635-µm (25 mil)-thick alumina substrates (Ceramtec, Rubalit 708S, 96 %), a semi-automatic screen-printing machine (Ami Presco 485) was used. All thick films with the exception of the silver paste were screen-printed one time. The samples were levelled at room temperature and dried at 150 °C for 10 min. Only the films produced from the pure silver paste were produced using four consecutive print/dry/fire processing cycles to achieve the required thickness. A sintering profile was applied to all of the samples according to the standard firing profile provided by the paste suppliers with a peak temperature of 850 °C and a dwell time of 10 min. After sintering, the samples were further processed as described below.

The widest lines of the test pattern were contacted by gap welding platinum wires on the metallization pads (Unitek Peco, Thinline Series 80). To mechanically fix the wires, a drop of platinum paste was added onto the wire pad interface. The samples were mounted in an alumina sample carrier and the welded wires were attached to the platinum wires of the sample holder. The sample holder was mounted in a tube furnace, which consists of an enclosed alumi-

na tube with a heating coil. During heating, it was purged with compressed air. As shown in Fig. 1, a 4-wire technique was used to neglect the resistance of the leads.
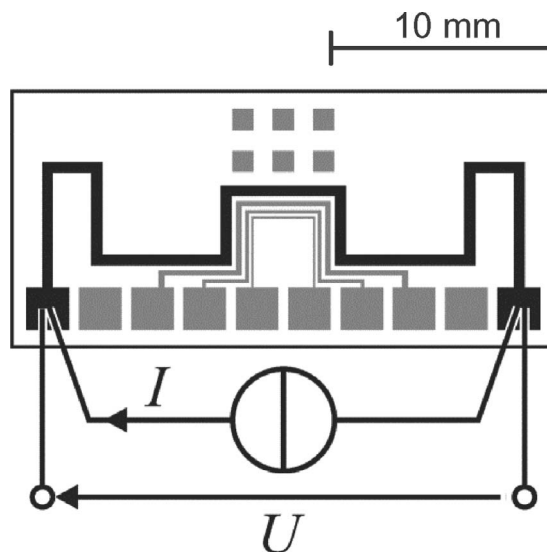

Fig. 1: Test structures used for all measurements shown in this paper according to DIN 41580 – 2.

The furnace temperature was controlled using a thermocouple with a distance to the sample of less than one millimeter. A second thermocouple, which was used to measure the temperature with a digital multimeter (Keithley 2700 data acquisition card 7700), was placed right next to the control thermocouple. This ensured that measurement and control temperature had the same value. The digital multimeter recorded also the resistance in a four-wire connection. In order to compensate thermoelectric voltages, an offset correction was performed [24].

In the following, a complete measuring procedure including 14 sintering cycles was applied, as shown by way of example for one sample in Fig. 2. When the temperature dropped below 50 °C, the next 850 °C-cycle was started. During the whole measurement, the tube furnace was purged with compressed air to ensure the same conditions as used for sintering of thick-film hybrids in oxidizing atmosphere. The resistance followed the temperature as can be seen in Fig. 2.

Table 1: Investigated commercial thick-film pastes and the basic properties taken from the manufacturers' datasheets.

| Material	Ag	Au	AgPt	AgPd
Manufacturer	Heraeus	DuPont	DuPont	DuPont
Identifier/type	LPA410 – 026	QG150	9770	6119
Mixing ratio (by weight)	not applicable	not applicable	100:1	2.5:1
Solid content in wt%	89.5 – 92.5 %	-	-	-
Fired film thickness (FFT) in µm	15 – 20	5	15 – 20	13 – 15
Square resistance in mW at FFT[1]	≤ 1.2 at 40 µm	< 5 at 10 µm	2 – 3 at 20 µm	25 – 35 at 15 µm
Resolution in µm lines/spaces	75/75	75/75	175/175	150/150

1) FFT = Fired Film Thickness
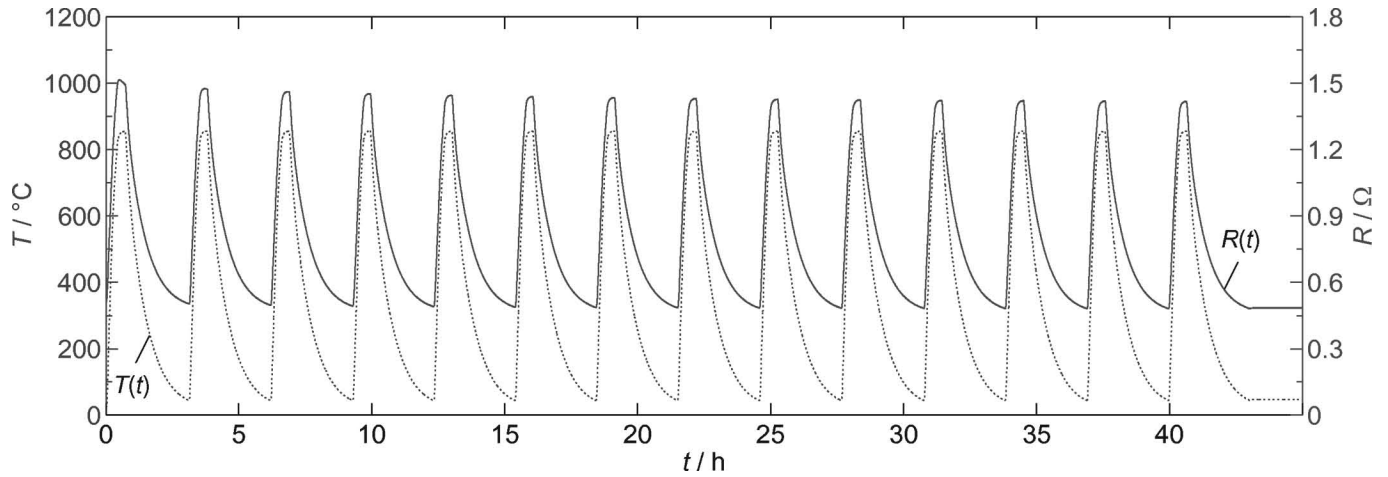
Fig. 2: Electrical resistance (solid line) during 14 subsequent sintering steps. The temperature is represented by the dotted line.

III. Results

(1) Electrical measurements

The resistance values were determined at 50 °C and at 850 °C for each single temperature cycle. The evaluation of discrete values had not supplied conclusive results. Therefore, resistance values for both temperatures have been averaged over a range of values. For this purpose, target temperature values had been defined (50 °C and 850 °C). Then, the measurement points were determined using a threshold value (5 °C). The average value then was calculated from the corresponding resistance values of these measuring points, as shown schematically in Fig. 3.
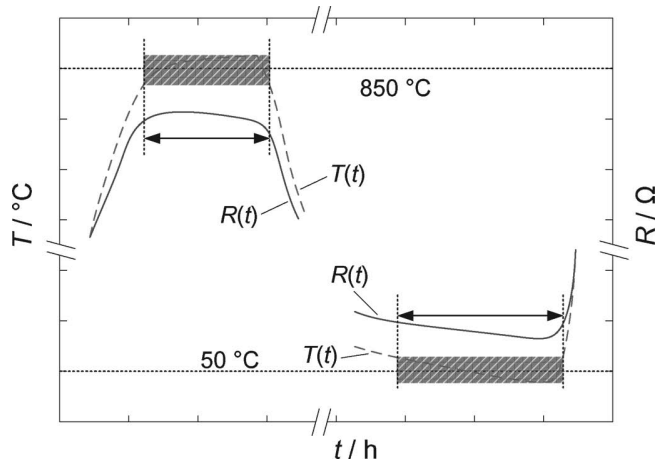

Fig. 3: To determine the resistor values to be considered, the simultaneously recorded temperature values were used. For both target temperatures (50 °C and 850 °C), those values were used which are localized in a band around the target values defined by the threshold (striped area).

In this manner, resistance values for $T = 50$ °C and $T = 850$ °C were obtained. In order to ensure the repeatability of the measurement results, this was conducted for a total of three samples for each paste. All resistance values were normalized to the respective first measured value. The obtained resistance values at 50 °C in dependence of the sintering cycle for all of the measured pastes can be seen in Fig. 4. All of them seem to asymptotically approach a limit value, whereas the resistance values of all

pastes except the silver-palladium paste decrease in dependence of the sintering cycles. It shows an increased resistance. When repeatedly sintered, printed metallization layers normally tend to compact, leading to decreased resistance. Furthermore, progressive sintering of the metal particles and purification of the metal layer caused by ongoing diffusion of the glass frit from the metallization layer to the alumina substrate during consecutive processing also causes a reduction of the resistance, especially for pastes with a high silver content [25]. Thick-film and LTCC resistors show a similar behavior. Coleman identified that the change in resistance of thick-film resistor systems during thermal aging is caused by three distinct mechanisms, corrosion, diffusion and compaction [26]. It can be described as a function of time t and temperature T by

$$\frac{\Delta R}{R_0} = \sum_i A_i t^{n_i} \cdot e^{\left(\frac{E_i}{kT}\right)} \qquad (1)$$

where A_i denotes a pre-exponential constant of each particular aging mechanism, n_i describes the time dependence, and E_i the corresponding activation energy. Using this approach, Dziedzic and Nowak were able to describe the resistance change of different thick-film resistors in dependence of time and temperature [20].

In this study, corrosion was neglected, because the long-term aging processes at elevated temperatures have not been evaluated. We fitted the values of relative resistance change R/R_0 in dependence of the sintering cycle using a decreasing exponential function

$$y(n) = A_1 \cdot e^{\frac{n}{t_1}} + A_2 \cdot e^{\frac{n}{t_2}} + y_0 \qquad (2)$$

containing two terms in order to describe the two processes that are considered to take place, compacting and purification (diffusion). A_1 and A_2 represent the amplitudes and t_1 and t_2 the decay constants for the two processes. n is the sintering cycle and y_0 is the offset corresponding to the final value of R/R_0 to which it is running asymptotically.
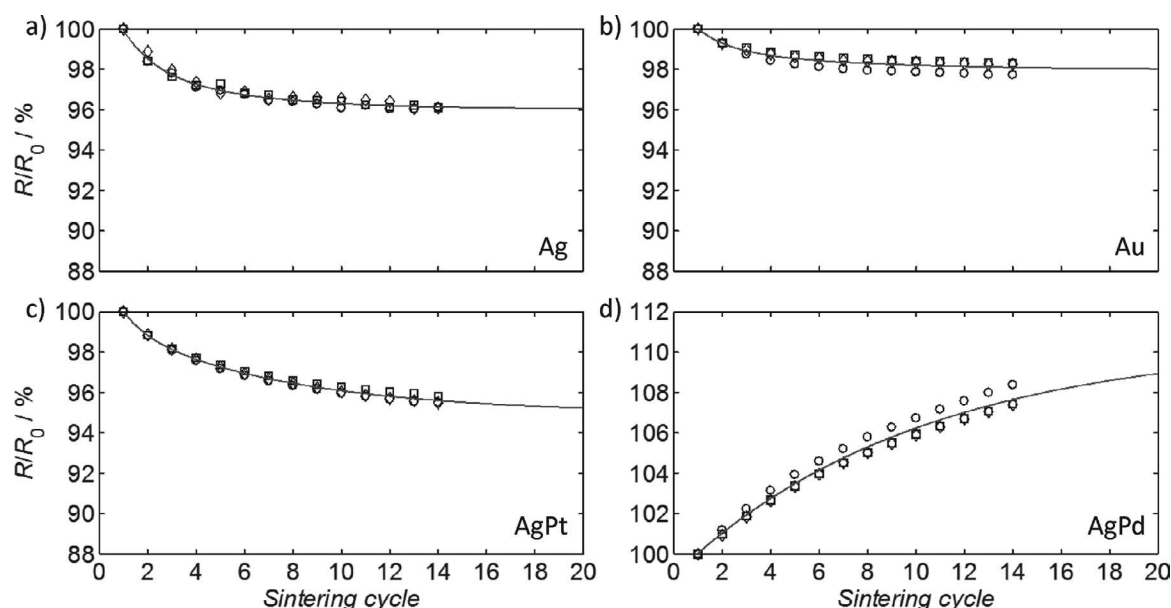
Fig. 4: The normalized averaged relative resistance change at 50 °C depends on the number of sintering cycles. The resistance of all pastes (a-c) decreases in dependence of sintering cycles, only the resistance of the silver-palladium paste rises with increased number of sintering cycles (d).

The resistance of the pure silver paste (Fig. 4a) decreases by 3.9 % over 14 sintering cycles. The lower limit of the resistance as a function of sintering cycles was calculated with the use of Eq. (2) to be 96.0 % of the initial value. The pure gold paste shows the slightest change in resistance as a function of sintering steps with a decrease in the resistance of only 1.9 % after the 14th sintering cycle (Fig. 4b). The lower limit respectively has been calculated to be only 98.0 % of the initial value. The decrease in the resistance of the platinum-alloyed silver paste amounts to 4.4 %. This resistance decrease is only slightly higher compared to the pure silver paste and a final value of 95.0 % was calculated (Fig. 4c). All values, including the fit parameters, are listed in Table 2. In contrast, the silver-palladium paste behaves differently. Unlike all other thick-film pastes, silver-palladium shows a resistance increase. The obtained values at 50 °C increase with the number of sintering steps to about 7.7 % of the initial value, as can be seen from Fig. 4d. It is likely that the increase in the resistance of the silver-palladium layers is related here to the well-known influence of oxygen in the sintering atmosphere and its influence on the redox system Ag-Pd-O [27,28,29,30]. Furthermore the calculated final value y_0 is calculated to be 123.9 %.

The temperature coefficient of resistance, *TCR*, has to be considered especially when the electrical circuit is used at elevated temperatures either from the periphery or dissipated heat to ensure the proper function of the circuit [6].

The *TCR* was calculated from the determined resistance values at $T = 50$ °C and $T = 850$ °C from the previously shown resistance data. If one assumes resistance changes that are directly proportional to temperature changes, it is sufficient to calculate only the 1st order *TCR* according to Eq. 3.

$$TCR = \frac{1}{R(50°C)} \cdot \frac{dR(T)}{dT} \qquad (3)$$

As shown in Fig. 5 the relationship between temperature and resistance is sufficiently linear. Illustrated is the resistance as function of temperature for the first and the last

sintering cycle. It can be assumed that this linear behavior is equally valid for the sintering cycles in between and a *TCR* can be defined (Eq. (4)):

$$TCR = \frac{1}{R(50°C)} \cdot \frac{R(850°C) - R(50°C)}{850°C - 50°C}. \qquad (4)$$

Table 2: Measured drops in resistance R/R_0 in % after 14 repeated firing cycles and calculated final value of resistance y_0 in %. Additionally, the calculated values of the fit parameters A and t are given.

Material	Ag	Au	AgPt	AgPd
R/R_0 in % measured	-3.9	-1.9	-4.4	7.7
y_0 in %	96.0	98.0	95.0	123.9
A_1	2.6	1.1	4.6	-3.6
t_1	4.4	6.2	7.2	-1.7
A_2	4.0	2.3	2.7	-22.7
t_2	1.3	1.3	1.0	-28.9

The resulting *TCR*-values in dependence of the sintering cycle are illustrated in Fig. 6. The first sintering cycle cannot be evaluated, because the platinum paste drop that mechanically fixes the wires also has to be sintered. Consequently, *TCR*-values are available starting from the second sintering cycle. For each paste, the mean over the three samples has been calculated. As expected from Matthiesen's rule, the *TCR* of the pure metals is higher than the silver paste with 1 % impurity (Pt). The silver palladium alloy shows a by far lower *TCR* below 400 ppmK⁻¹. The *TCR* of the silver layer and the gold layer increased during the first five examined sintering steps by about 55 ppmK⁻¹ and 34 ppmK⁻¹, respectively, and thereafter remained constant (Fig. 6a and Fig. 6b). The *TCR* of the silver-platinum layer shows a lower dependence

on the number of sintering steps in the considered interval with an increase of only about 17 ppmK^{-1} (Fig. 6c). The determined values of the *TCR* of the silver-palladium films show a different behavior, analogous to the resistance measurements. On the one hand, a decrease occurs with increasing number of sintering cycles, on the other hand the absolute values of change of *TCR* are much lower with a value of 14 ppmK^{-1} (Fig. 6d). The relative change of *TCR* of the silver-palladium paste with 4 % is the highest of the investigated pastes. A change of *TCR* after the fifth sintering step, however, does not occur even in the case of the silver-palladium paste. All values are listed in Table 3.

Table 3: TCR before and after 14 temperature cycles. TCR_1 is the TCR after the first and TCR_{14} is the *TCR* after the 14th sintering cycle.

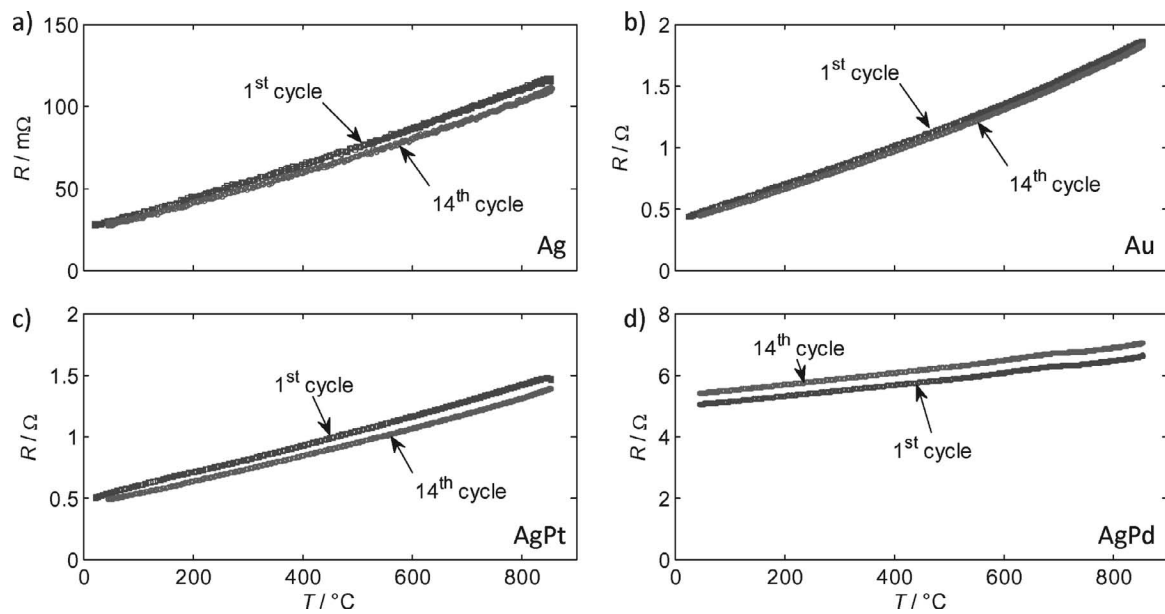| Material	Ag	Au	AgPt	AgPd
TCR_1 in ppmK^{-1}	3564	3580	2262	387
TCR_{14} in ppmK^{-1}	3618	3613	2280	374
ΔTCR in ppmK^{-1}	55	34	17	-14
ΔTCR in %	2	1	1	-4

Fig. 5 : The resistance of the pastes depends linearly on temperature. The pure silver and gold pastes and the platinum-alloyed silver paste show decreased resistance after the fourteenth sintering cycle compared to the first one (a-c), in contrast to the palladium-alloyed silver paste, which shows the opposite behavior (d).
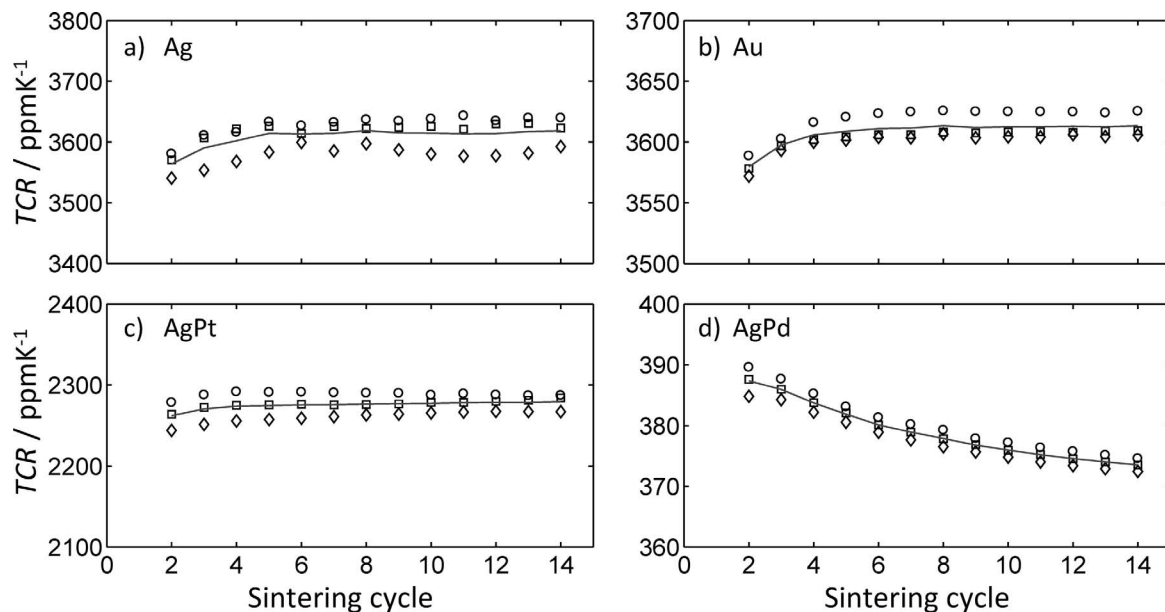

Fig. 6: The *TCR* of the pure silver and gold pastes and the platinum-alloyed silver paste increase with proceeding sintering (a-c), in contrast to the palladium alloyed silver paste (d). Measured values are represented by symbols, the calculated mean by lines.

(2)   Ceramography and analyses

The question arises whether the changes in resistance and *TCR* are reflected also by ceramographic images and SEM-EDX analyses of the layers. In particular the diffusion of paste components into the ceramic substrate was investigated using SEM images (Zeiss LEO 1450 VP) and EDX measurements (Oxford Instruments INCA Energy 300). All analytical measurements are based on samples that were produced according to those used for the electrical measurements. In order to obtain cross-sections of the metallization layers for each sintering step, an approximately 2.5-mm-thin slice was separated from the test substrates after each sintering step. The samples were prepared deformation-free using a precision table-top cut-off machine (Struers Accutom 50). In the following, the isolated samples were embedded in a cold curing epoxy resin system under vacuum. So preparation artifacts were avoided, as these could affect the EDX studies. To prepare the samples for optimum EDX studies, the embedded samples were ground and polished with semi-automated grinding and polishing apparatus (Tegrapol-11, TegraForce-1, Tegra-Doser-1).

(3)   Diffusion depth

Recorded SEM images were analyzed with the help of the photo-editing software "Analysis". By defining reference points on the contour of the interface between the substrate and the conductor track, the path of the interface surface was approximated according to line a) in Fig. 7. The same procedure was used to define the depth of diffusion. Here, the reference points were defined on the basis of the brighter zone shown in the alumina substrate. Inhomogeneities of the grain size distribution in the alumina substrate caused a partially uneven course of the diffusion zone, as can be seen in line b) in Fig. 7. In the next step, a so-called neutral fiber was inserted (dotted line c in Fig. 7). It is calculated by the software iteratively by adjusting the normals of the neutral fiber. The bases of the neutral fiber were calculated to halve the length of the normals between conductor-substrate interface and boundary of the diffusion zone. Then the diffusion depth was calculated by determining the lengths of each of the normals and calculating their average value.

In Fig. 8, the results obtained for all paste systems are shown. For all four conductor pastes an increase in the diffusion zone with an increasing number of sintering steps is found. Caused by the four printing and sintering steps, which are necessary to achieve the thickness of the thick-silver layer, the first measurement point appears at the fourth sintering cycle.

The data can be fitted according to a parabolic law, as it is typical for diffusion-controlled processes. In Eq. 4, K is a constant dependent on the material system and the process parameters at a given constant temperature; t denotes the sintering step. It has no unit and can be seen as proportional to the number of sintering steps, n, with duration of ten minutes each and thus takes the place of the time parameter. z is the diffusion depth and z_0 is an offset, which is necessary in this case to provide the fit despite the abrupt increase of the penetration depth after the first sintering step. This approach arises from the fact that it is not directly the diffusion over a period of time that is considered, but the extension of diffusion regions after repeated ten minutes of sintering.

$$z = K \cdot \sqrt{t} + z_0 \qquad (5)$$

The parabolic law can be calculated assuming a constant concentration gradient from the first Fick's law [31]. All values of diffusion depth have been rounded to a precision of 1 μm and are summarized in Table 4, including the fit parameters

Table 4: Measured values of diffusion depth after 14 sintering cycles and obtained parameters for the parabolic law in Eq. 3.

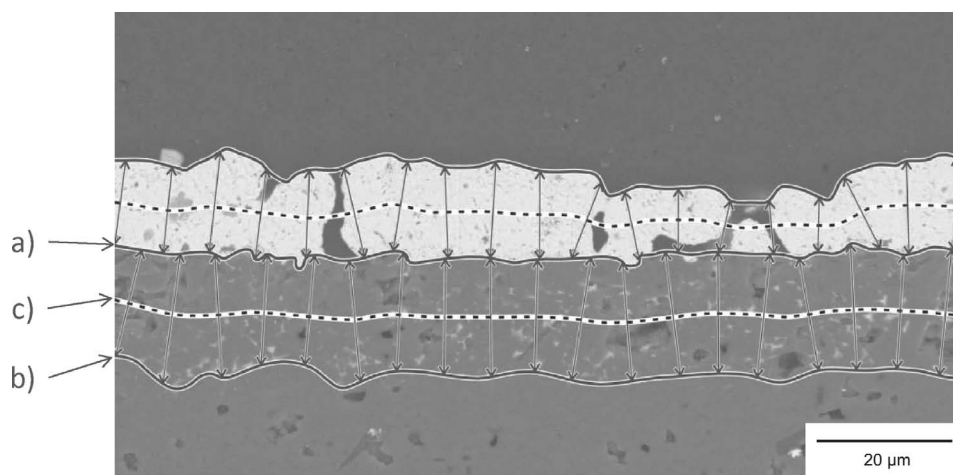| Material	Ag	Au	AgPt	AgPd
K in μm	7.9	0.72	2.8	6.3
z_0 in μm	0.35	1.8	8.7	7.5

Fig. 7: Measurement of the diffusion depth illustrated in a cross-section micrograph. The diffusion depth is the mean of the distances (arrows) between the interface of conductor track and substrate (line a) and the diffusion front in the substrate (line b). Line c is the so-called neutral fiber. It is calculated to halve its normals (arrows).

It is important to note that on the basis of the optically determined diffusion zone at this point, no information on the diffused substances or elements can be obtained. This will be explored further below with reference to the EDX results. Owing to the four-time printing of the pure silver layers, the diffusion depth of the silver layers could be evaluated only from the fourth sintering step. After the 14th sintering step, a diffusion depth of 29 µm was determined. However, it exhibits a good match with the parabolic growth law as shown in Fig. 8a. As can be seen in Fig. 8b, the layers of the pure gold paste show by far the lowest diffusion depth among the examined pastes. The diffusion depth after the 14th sintering step was found to be only 5 µm. The investigated layers of the silver-platinum paste show lower values than the films of the pure silver paste, the diffusion depth was determined to be 19 µm (Fig. 8c). The results of the diffusion depth of the layers of the silver-palladium paste, however, again show a different behavior. Almost the same values of the diffusion depth

were obtained as for the layers of pure silver paste. The determined diffusion depth after the 14th sintering step reached 31 µm, representing the largest penetration of all investigated paste systems (Fig. 8d).

(5) EDX results

To quantitatively determine the elements that can be found in the diffusion zone, the samples of the first and the 14th sintering step were examined by means of EDX; the silver-platinum conductor tracks shall serve as an example. Elements with high atomic number will cause more backscatter than those with lower atomic number. Therefore, areas that contain these elements appear brighter in SEM image. The grain boundaries represent distortions and allow the necessary concentration gradients for side exchange processes. This can be seen in the SEM image in Fig. 9. The diffusion in the polycrystalline Al_2O_3 substrate mainly takes place along the grain boundaries (bright regions).
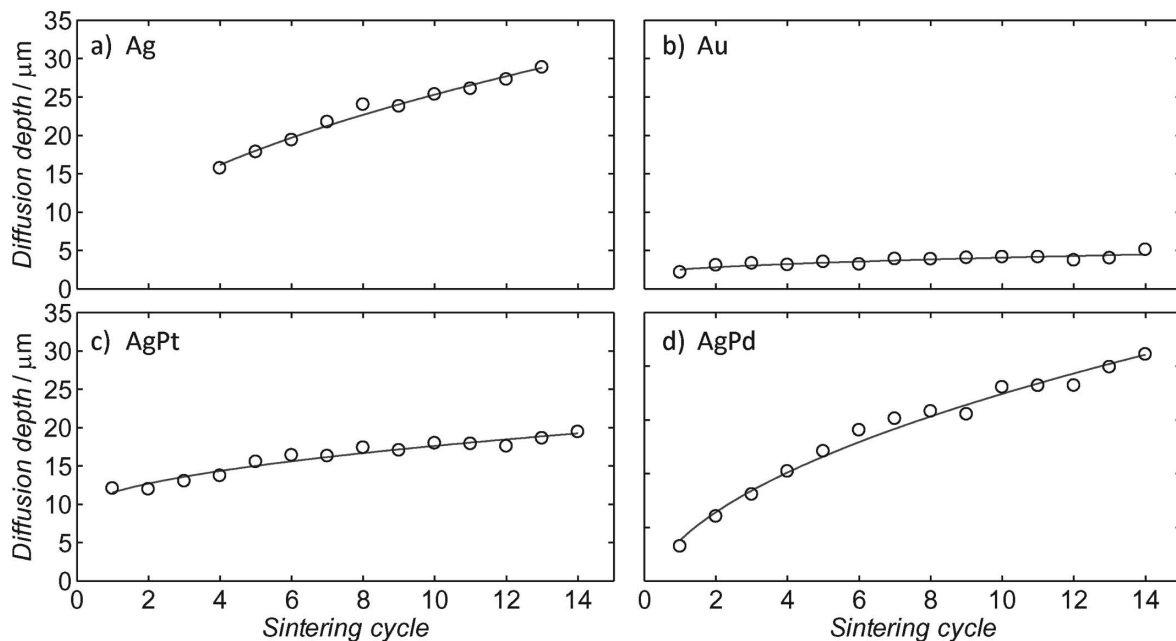

Fig. 8: Diffusion depths of the four investigated paste systems in dependence of the sintering cycles (dots). The solid line in each case represents the fit according to the parabolic growth law. The fit parameters can be obtained from Table 4.
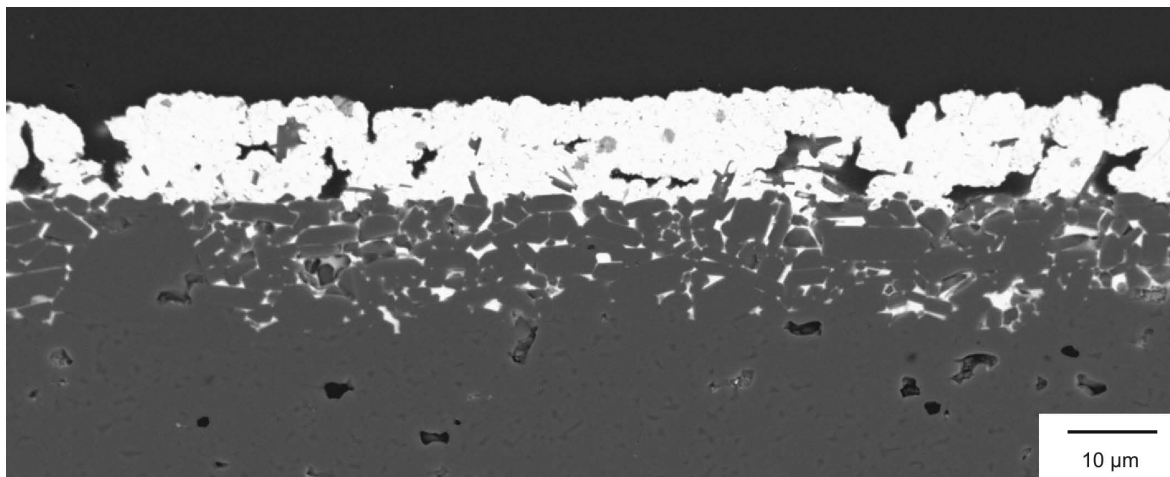

Fig. 9: The diffusion in the polycrystalline Al_2O_3 substrate mainly takes place along the grain boundaries (bright regions), as shown for silver-platinum after the first sintering cycle.
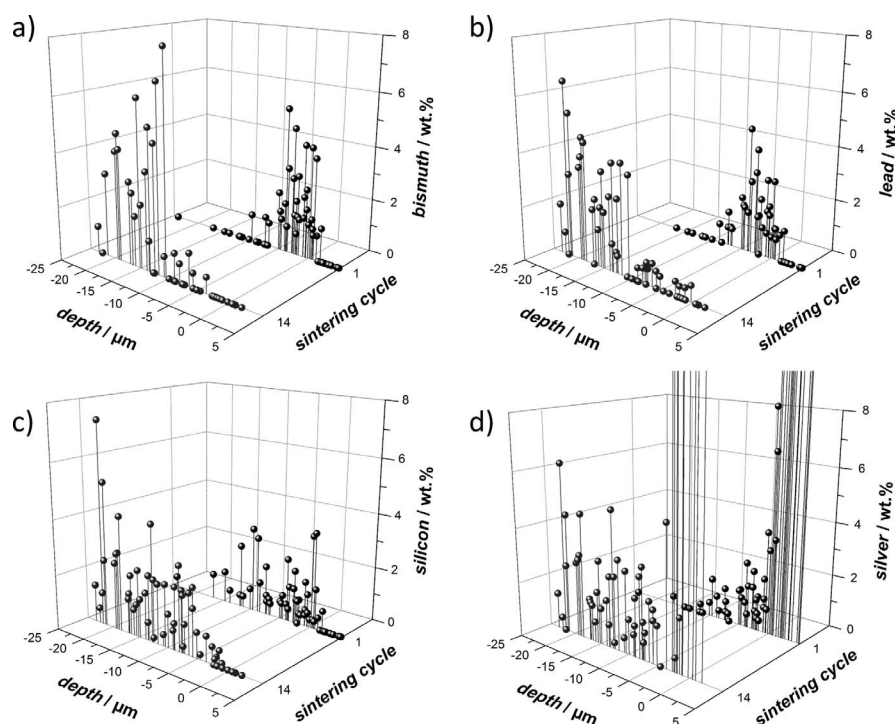
Fig. 10: EDX results on grain boundaries in the diffusion zone beneath the silver-platinum layer at sintering step 1 and 14. Representation of the determined amounts of bismuth (a), lead (b), silicon (c) and silver (d).

EDX spot measurements were therefore conducted on the light-appearing grain boundaries. A search was made for the expected elements, originating from the glass frit such as lead, bismuth, and silicon, and the metallic paste components were also searched for. For the elements bismuth, lead and silicon, a change in concentration between the first and the 14th step of the sintered substrate was detected. Also the diffusion of silver was detected. However, platinum could not be detected because the percentage in the film was below the EDX detection limit. All results are shown in Fig. 10. The zero point in each case represents the transition from the metallization to the substrate. Negative values therefore refer to locations within the substrate.

After the first sintering cycle, increased concentrations of the examined items in the measured substrate were detected. As can be seen from Fig. 10a and Fig. 10b, bismuth and lead diffused about 10 µm deep. Silicon is detected at even greater depths, as shown in Fig. 10c. Since the here-used Al_2O_3 substrates contain approximately 3 wt% silicon, the measured values cannot be connected directly to the diffusion of silicon from the glass frit at the first sintering step. Bismuth and lead are added as Bi_2O_3 and PbO to the pastes in small amounts. They serve as a flux, which explains the high diffusivity. After the 14th temperature cycle the element contents of bismuth and lead in a depth between 0 µm and 10 µm have decreased against zero, while at a greater depth, starting at 10 µm up to 25 µm from the transition from the metallization to the substrate a higher content of the elements up to 6 % has been detected. The diffusion front has moved into the substrate while the source of the elements, the glass frit in the metallization, has decreased. This is typical for diffusion from an exhaustible source and means that the components of the glass frit have diffused nearly completely into the ceramic substrate.

For silicon, despite the superposition of the Si-content of the substrate, a similar trend is discernible. The amount of silicon got slightly higher and an increase in concentration was detected up to 24 µm deep. Silver reached a diffusion depth of about 13 µm (Fig. 10c) after the first sintering step. This value agrees with the averaged measurement point for the first sintering step in Fig. 8a. The diffusion profile represents a typical profile obtained for diffusion from an inexhaustible source. This can be explained by the high silver content of the silver-platinum paste.

(6) Correlation

In the last step it was investigated how the relative change in resistance and the diffusion depth correlate. Fig. 11 shows the results summarized for each paste. It becomes clear that in the case of high absolute value of the relative change in resistance, a large diffusion depth also occurs. Nevertheless, the layers of the individual pastes showed slight deviations from each other. The layers of pure silver paste showed a relatively small relative change in resistance of 4.0 % at a comparatively high diffusion depth of 29 µm. The layers of pure gold paste simultaneously have a very small change in relative resistance and the diffusion depth. Thus, even after the 14th sintering cycle, a relative change in resistance of only 2.0 % is obtained at a diffusion depth of only 5 µm. According to the results shown above, the silver-platinum paste shows a slightly bigger change in relative resistance with a value of 5.0 %. At the same time, with 19 µm a considerably lower diffusion depth than for the layers of pure silver paste was observed. In the case of silver-palladium paste, the correlation between relative change in resistance of the layers and the diffusion depth is especially marked. After the 14th sintering cycle, the relative resistance was 8.8 % and a diffusion depth of 31 µm was observed.
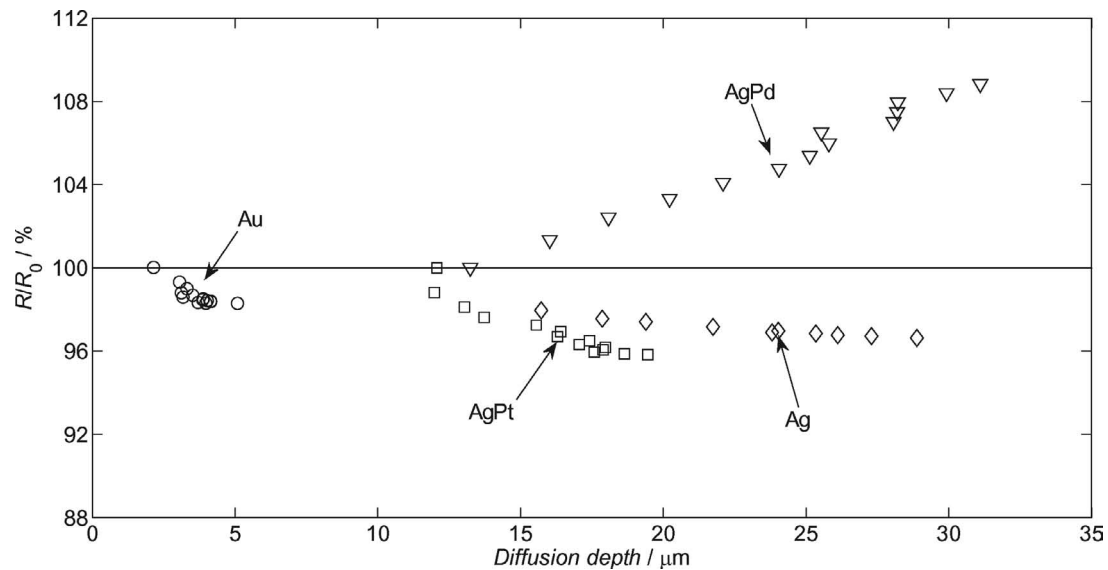
Fig. 11: A relationship between the relative change in resistance and the diffusion depth can be observed, which is approximately linear for all pastes. A small change of the relative change in resistance is also associated with a small diffusion depth. Silver-palladium shows the largest change in resistance and at the same time the greatest diffusion depth.

IV. Conclusions and Outlook

In this work, the effect of repeated sintering cycles on the electrical properties of screen-printed thick films produced from four commercial thick-film pastes has been investigated. Typical pastes show a decrease of resistance and an increase in *TCR*, while the silver-palladium paste shows the opposite behavior. The values of the relative change in resistance correlated with the particular diffusion depth for all four pastes. Knowing the observed correlations, the measured material properties determined after single sintering can be transferred to repeatedly sintered thick films.

Similar relationships as between relative change in resistance and diffusion depth can be expected also for the change in porosity and the change in thickness, which is equivalent to the sintering progress of the layers leading to compacter films. Future work will include the evaluation of film thickness and determination of porosity. Therefore, it would be necessary to determine the thickness of the printing layers at exactly the same place. To determine the porosity, the pore surface can be determined with the nitrogen adsorption method. Burnside *et al.* applied both methods to thick films [32].

References

[1] Prudenziati, M.: Thick-film technology, *Sensor. Actuat. A*, **25–27**, 227–234, (1991).

[2] White, N.M., Turner, J.D., Thick-film sensors: past, present and future, *Meas. Sci. Technol.*, **8**, 1–20, (1997).

[3] Bartsch de Torres, H., Rensch, C., Fischer, M., Schober, A., Hoffmann, M., Müller, J.: Thick film flow sensor for biological microsystems, *Sens. Actuat. A*, **160**, 109–115, (2010).

[4] Schubring, A., Sarma, D.H.R., Webster, M.E.: Wirebonding on multilayer circuits for automotive applications using robust thick-film conductors, In: Proceedings of the 1998 International Symposium on Microelectronics, San Diego, CA., 1998

[5] Fairchild, M.R., Snyder, R.B., Berlin, C.W., Sarma, D.H.R.: Emerging substrate technologies for harsh-environment automotive electronics applications, SAE Technical Paper 2002–01–1052, (2002).

[6] Ortolino, D., Kita, J., Wurm, R., Blum, E., Beart, K., Moos, R.: Investigation of the short-time high-current behavior of vias manufactured in hybrid thick-film technology, *Microelectron. Reliab.*, **34**, 1257–263 (2011)

[7] Moos, R.: A brief overview on automotive exhaust gas sensors based on electroceramics, *Int. J. Appl. Ceram. Technol.*, **2**, 401–413, (2005).

[8] Riegel, J., Neumann, H., Wiedenmann, H.-M.: Exhaust gas sensors for automotive emission control, *Solid State Ionics*, **152–153**, 783–800, (2002).

[9] Naguib, H.M., MacLaurin, B.K.: Silver migration and the reliability of Pd/Ag conductors in thick-film dielectric crossover structures, *IEEE T. Compon. Hybr.*, **2**, 196–207, (1979).

[10] Lienig, J., Jerke, G., Adler, T.: Electromigration avoidance in analog circuits: two methodologies for current-driven routing, Proceedings of the 15th International Conference on VLSI Design (VLSID 02), Bangalore, India, 2002

[11] Jerke, G., Lienig, L.: Hierarchical current-density verification in arbitrarily shaped metallization patterns of analog circuits, *IEEE T. Comput. Aid. D.*, **23**, 80–90, (2004).

[12] Lin, J.-C., Chuang, J.-Y.: Resistance to silver electrolytic migration for Thick-Film conductors prepared from mixed and alloyed powders of Ag-15Pd and Ag-30Pd, *J. Electrochem. Soc.*, **144**, 1652–1659, (1997).

[13] Cawley, J.D., Lee, W.E.: Oxide ceramics. materials science and technology, John Wiley & Sons, Ltd, 2006.

[14] Reichl, H.: Hybrid integration: technology and design of thick-film circuits, (in German), Dr. Alfred Hüthig Verlag GmbH, 1988

[15] Cattaneo, A., Cocito, M., Forlani, F., Prudenziati, M.: Influence of the metal migration from Screen-and-fired terminations on the electrical characteristics of thick-film resistors, *Electrocomponent Sci. Technol.*, **4**, 205–211, (1977).

16 Yajima, K.-I., Yamaguchi, T.: Sintering and microstructure development of glass-bonded silver thick films, *J. Mater. Sci.*, **19**, 777 – 784, (1984).

17 Yajima, K.-I., Yamaguchi, T.: A further study on the microstructure of glass-bonded ag thick-film conductors, *IEEE T. Compon. Hybr.*, **7**, 281 – 285, (1984).

18 Lin, J.C., Wu, W.: On the sintering of mixed and alloyed silver-palladium powders from chemical coprecipitation, *Mater. Chem. Phys.*, **40**, 110 – 118, (1995).

19 Rane, S.B., Seth, T.G., Phatak, J., Amalnerkar, D.P., Das, B.K.: Influence of surfactants treatment on silver powder and its thick films, *Mater. Lett.*, **57**, 3096 – 3100, (2003).

20 Lin, J.C., Wang, C.Y.: Effect of surface properties of silver powder on the sintering of its thick-film conductor, *Mater. Chem. Phys.*, **45**, 253 – 261, (1996).

21 Dziedzic, A., Nowak, D.: Thick-film and LTCC passive components for high-temperature electronics, *Radioengineering*, **22**, 218 – 226, (2013).

22 Zhang, R., Johnson, R.W., Vert, A., Zhang, T., Shaddock, D.: Failure mechanism in thick film materials for 300 °C operation, *IEEE T. Compon. Pack.*, **2**, 1750 – 1758, (2012).

23 Nowak, D., Stafiniak, A., Dziedzic, A.: Analysis of electromigration phenomenon in thick-film and LTCC structures at elevated temperature, *Mater. Sci. Poland*, **32**, 247 – 251, (2014).

24 Model 2700 Multimeter/Switch System, User's Manual, Keithley Instruments, Issue 2700 – 900 – 01 Rev. F (2002) S. 121 ff.

25 Taylor, B.E., Felten, J.F., Larry, J.R.: Progress in and technology of low-cost silver containing thick-film conductors, *IEEE T. Compon. Hybr.*, **3**, 504 – 517, (1980).

26 Coleman, M.: Ageing mechanisms and stability in thick film resistors, *Microelectron. Int.*, **1**, 36 – 41, (1984).

27 Wang, S.F., Huebner, W., Huang, C.: Correlation of subsolidus phase relations in the Ag–Pd–O system to oxidation reduction kinetics and dilametric behavior, *J. Am. Ceram. Soc.*, **75**, 2232 – 2239, (1992).

28 Cole Jr, S.S.: Oxidation and reduction of palladium in the presence of silver, *J. Am. Ceram. Soc.*, **68**, 106 – 107, (1985).

29 Szafránski, A.W.: Influence of hydrogen on electron transport of palladium alloyed with silver, *J. Alloy. Compd.*, **395**, 36 – 40, (2005).

30 Garino, T., Rodriguez, M.: Behavior of silver and palladium mixtures during heating, *J. Am. Ceram. Soc.*, **83**, 2709 – 2714, (2000).

31 Merkel, M., Thomas, K.-H.: Materials manual, (in German). 7th edition. Carl Hanser Verlag, 2008, S. 130 ff.

32 Burnside, S. *et al.*: Deposition and characterization of screen-printed porous multi-layer thick film structures from semiconducting and conducting nanomaterials for use in photovoltaic devices, *J. Mater. Sci. - Mater. Electron.*, **11**, 355 – 362, (2000).